HHS Public Access

Author manuscript

Gastroenterology. Author manuscript; available in PMC 2024 November 01.

Published in final edited form as:

Gastroenterology. 2023 November ; 165(5): 1136–1150. doi:10.1053/j.gastro.2023.07.017.

Ceramides increase fatty acid utilization in intestinal progenitors to enhance stemness and increase tumor risk

Ying Li[1,†], **Bhagirath Chaurasia**[1,2,*,†], **M. Mahidur Rahman**[3,†], **Vincent Kaddai**[1], **J. Alan Maschek**[1], **Jordan A. Berg**[4], **Joseph L. Wilkerson**[1], **Ziad S. Mahmassani**[5], **James Cox**[4], **Peng Wei**[4], **Peter J Meikle**[6], **Donald Atkinson**[1], **Liping Wang**[1], **Annelise M. Poss**[1], **Mary C. Playdon**[1], **Trevor S. Tippetts**[1], **Esraa M. Mousa**[1,7], **Kesara Nittayaboon**[1,8], **Pon Velayutham Anandh Babu**[1], **Micah J. Drummond**[5], **Hans Clevers**[9], **James A Shayman**[10], **Yoshio Hirabayashi**[11], **William L. Holland**[1], **Jared Rutter**[4,12], **Bruce Edgar**[3], **Scott A. Summers**[1,*]

[1]Department of Nutrition and Integrative Physiology and the Diabetes and Metabolism Research Center, University of Utah, 15 North 2030 East, Salt Lake City, UT 84112

[2]Division of Endocrinology, Department of Internal Medicine, Fraternal Order of Eagles Diabetes Research Center, University of Iowa

[3]Huntsman Cancer Institute and Department of Oncological Sciences, University of Utah, Salt Lake City, UT 84112, USA

[4]Department of Biochemistry, University of Utah, Salt Lake City, UT 84112

[5]Department of Physical Therapy and Athletic Training, University of Utah

[6]Baker Heart and Diabetes Institute, Melbourne, Australia

[7]Tanta University, Egypt

[8]Prince of Songkla University, Thailand

[9]Hubrecht Institute, Royal Netherlands Academy of Arts and Sciences (KNAW) and UMC Utrecht, 3584 CT Utrecht, the Netherlands; Oncode Institute, Hubrecht Institute, 3584 CT Utrecht, the Netherlands; The Princess Maxima Center for Pediatric Oncology, 3584 CS Utrecht, the Netherlands

[*]**Address for correspondence** Scott Summers, PhD, Department of Nutrition and Integrative Physiology and the Diabetes and Metabolism Research, Center, University of Utah, 15 North 2030 East, Salt Lake City, UT 84112, Scott.a.summers@health.utah.edu Bhagirath Chaurasia, PhD, Division of Endocrinology, Department of Internal Medicine, Fraternal Order of Eagles Diabetes, Research Center, University of Iowa, IA 52242, bhagirath-chaurasia@uiowa.edu.

[†]Authors contributed equally

Author contributions

S.A.S, B.C., and Y.L. conceived of the project, designed the experiments, and wrote the initial draft of the manuscript. Y.L, B.C, M.R., V.A.K., J.B., J.L.W., Z.M., P.W., D. A., L.W., A.M.P., M.C.P., T.S.T performed experiments and analyzed data. P.V.A.B., M.D., C.B, J.R, H.C, Y.H, and J.A.S., and B.E. provided mouse strains or other critical reagents. J.L.W and W.L.H. assisted in the quantification of images. D.L provided human tissues used in this study and J.C, P.W and P.J.M aided in lipid analysis.

Conflict of Interests.

SAS is a founder and shareholder of Centaurus Therapeutics. LPW is a shareholder of Centaurus Therapeutics. None of the other authors have relevant conflicts relevant to this manuscript.

[10]Department of Internal Medicine, University of Michigan, Ann Arbor, Michigan 48109, USA

[11]Cellular Informatics Laboratory, RIKEN Cluster for Pioneering Research, RIKEN, Wako-shi, Saitama Japan

[12]Howard Hughes Medical Institute, Salt Lake City, UT 84112

Abstract

Background and Aims—Cancers of the alimentary tract including esophageal adenocarcinomas, colorectal cancers, and cancers of the gastric cardia are common comorbidities of obesity. Prolonged, excessive delivery of macronutrients to the cells lining the gut can increase one's risk for these cancers by inducing imbalances in the rate of intestinal stem cell proliferation vs. differentiation, which can produce polyps and other aberrant growths. We investigated whether ceramides, which are sphingolipids that serve as a signals of nutritional excess, alter stem cell behaviors to influence cancer risk.

Methods—We profiled sphingolipids and sphingolipid-synthesizing enzymes in human adenomas and tumors. Thereafter, we manipulated expression of sphingolipid-producing enzymes, including serine palmitoyltransferase (SPT), in intestinal progenitors of mice, cultured organoids, and *Drosophila* to discern whether sphingolipids altered stem cell proliferation and metabolism.

Results—SPT, which diverts dietary fatty- and amino-acids into the biosynthetic pathway that produces ceramides and other sphingolipids, is a critical modulator of intestinal stem cell homeostasis. SPT and other enzymes in the sphingolipid biosynthesis pathway are upregulated in human intestinal adenomas. They produce ceramides which serve as pro-stemness signals that stimulate peroxisome-proliferator activated receptor alpha and induce fatty acid binding protein-1. These actions lead to increased lipid utilization and enhanced proliferation of intestinal progenitors.

Conclusion—Ceramides serve as critical links between dietary macronutrients, epithelial regeneration, and cancer risk.

Lay summary

These studies demonstrate that ceramides, which are products of fat and protein metabolism, may link unhealthy diets to the formation of intestinal polyps that seed cancer.

Keywords

Stem cell; sphingolipids; ceramides; metabolism; colorectal cancer

Introduction

The intestinal epithelium is the most rapidly regenerating tissue in the body. Constant mechanical damage inflicted by passing bowel content necessitates the nearly complete renewal of the epithelium every 4–5 days [1]. Replacement of the intestinal villi results from a coordinated process triggered by the proliferation and differentiation of intestinal stem cells (ISCs) that lie in a crypt at the base of the villus. The ISCs give rise to the specialized absorptive cells (i.e., enterocytes) and mucus and hormone-secreting goblet and

enteroendocrine cells, respectively, that comprise the bulk of the villus epithelium. The balance between ISC proliferation and differentiation is tightly regulated and its disruption leads to gastroenteritis or the formation of hyperproliferative lesions that seed tumors.

ISCs respond to nutritional cues that increase proliferation and enhance the regenerative capacity of the gut epithelium. For example, the fatty acid palmitate stimulates proliferation of ISCs, thus increasing the number of cells within the crypt to enhance tumor risk [2]. By contrast, serine deprivation restricts the growth of intestinal cancers [3]. Since palmitate and serine are required to synthesize the sphingoid backbone of sphingolipids, we developed the hypothesis tested herein that one or more sphingolipids might be important signaling intermediates linking these dietary macronutrients to stem cell fate.

Once palmitate enters cells, it is quickly conjugated to coenzyme A, which traps the fatty acid in the cell and activates it for subsequent metabolism. The resultant palmitoyl-CoA can be coupled to (i) a glycerol backbone to produce glycerophospholipids, (ii) carnitine for transport into mitochondria, or (iii) the amino acid serine to generate sphingolipids. This latter serine conjugation step is catalyzed by serine palmitoyltransferase (SPT), which generates the sphingoid backbone present in sphingolipids. This moiety subsequently acquires additional, variable fatty acids and a critical double bond to form ceramides, which are the precursors of sphingomyelins and gangliosides (Figure 1A). Ceramides, particularly those containing a C_{16}-acyl chain, have emerged as important nutrient signals that alter cellular metabolism in response to excessive ectopic fatty acids [4]. Though sphingolipids are relatively minor components of the mouse gut lipidome [Figure 1B (jejunum) and S1A (colon), light blue] that are far less abundant than glycerolipids and sterols (Figure 1B, dark blue), the studies presented herein reveal that they are potent nutrient signals that alter the metabolism of ISCs to enhance stemness and accelerate epithelial regeneration.

Materials and Methods

Human colon samples

Human colon cancer tissues were obtained from the Preclinical Research Resource at the Huntsman Cancer Institute. Tumors were collected during tumor resection (not biopsies) and cryopreserved as viable tissue. The adjacent normal tissue was collected as a paired control.

Analysis of published human datasets for normal mucosa and adenomas

Microarray expression data were accessed and analyzed as described in a previous publication [5]. Additional details are in the supplemental methods.

Animal Colonies

The animal models and detailed treatment regimens are in the supplemental methods. All animal experiments were conducted with protocols approved by the Institutional Animal Care and Use Committee (IAVUC) of the University of Utah.

Lipidomics

Lipidomics was conducted mass spectroscopy at either the University of Utah Metabolomics Core[6] or the Baker Heart and Diabetes Institute[7]. Detailed methods are available in the supplementary materials.

Antibiotic treatment of *Sptlc2*$^{\delta IEC}$ mice

Antibiotic treatments were done as previously described[8]. Detailed methods are provided in the supplementary materials.

Quantitative RT-PCR

Quantitative RT-PCR was conducted as we described previously [6]. Additional details are provided in supplementary materials.

Histology and Immunochemistry

Histology and immunochemistry were conducted by ARUP Laboratories, Utah. Additional details are provided in the supplementary materials.

Isolation, culture, and analysis of intestinal organoids.

Detailed methods for organoid isolations are included in the supplementary materials. Cell death of organoid cultures was determined by propidium iodide (PI)-positive staining. Images were taken by EVOS digital inverted microscope. PI staining was quantified using Image J software (NIH).

FITC-Dextran Permeability Test

Intestinal permeability was assessed by oral gavage of FITC–dextran (Sigma-Aldrich, 46945–100MG-F, MW: 70,000). Mice were administered 500 μl FITC-Dextran (20mg/ml in PBS, 10mg/mouse) by gavage. Serum sample were collected 4-hours after oral gavage; Fluorescence were measured by a fluorescence plate reader at 488nm. Serum FITC-Dextran concentration was calculated according to the standard curve made by a serial dilution from the stock in PBS.

Fly stocks, maintenance, and experiments

Detailed descriptions of the Drosophila experiments are provided in the supplementary materials.

Isolation, culture, and analysis of intestinal organoids

Small intestinal crypts were isolated and grown into organoids as described previously [9]. Additional details are provided in the supplementary materials.

RNAseq and scRNA-seq Analysis.

RNAseq and scRNA-seq analysis was conducted at University of Utah genomics core facility. Additional details are provided in the supplemental methods.

Western Blot Analysis

Western blotting was conducted as described previously[6]. Additional details are provided in the supplementary materials.

Fatty Acid Uptake Assay

Fatty acid uptake was monitored using a QBT™ Fatty Acid Uptake Assay Kit, Molecular Devices. Details are provided in the supplementary materials.

RNA fluorescence *in situ* hybridization for mouse small intestine

Formalin-fixed paraffin-embedded (FFPE) mouse jejunum sections were de-paraffinized, rehydrated, and then hybridized with mRNA probes against mouse *Sptlc2, Olfm4* and *Lyz1* in accordance with the manufacturer's instructions (Advanced Cell Diagnostics, Newark, CA). In brief, FFPE sections were pretreated with hydrogen peroxide, incubated in Target Retrieval solution in a steamer for 30 minutes, and permeabilized by incubating in Protease Plus solution for 40 minutes. After hybridization, a fluorescent kit was used to amplify the mRNA signal. TSA Plus Fluorescein, TSA Plus Cyanine 3, and TSA Plus Cyanine 5 fluorescent signals were detected using EVOS digital inverted microscope.

PPAR Alpha Transcription Factor Activity Assay

The transcriptional activity of PPARα was assayed according to the manufacturer's guidelines (Abcam, ab133107). Additional details are provided in the supplemental methods.

Statistical analysis

Data were plotted as the mean ± SEM. Student *t*-test, one-way or two-way ANOVA were carried out using Excel or prism and statistical significance was considered meaningful at $p<0.05$.

Results

Sphingolipids and sphingolipid-synthesizing enzymes accrue in human intestinal adenomas

Colorectal cancers arise predominantly from precancerous adenomas. We interrogated two public gene expression datasets from early-stage human intestinal adenomas [10, 11], seeking to determine whether sphingolipid-synthesizing genes were differentially expressed in normal vs. adenomatous tissue. Transcripts encoding essential SPT subunits (*SPTLC1&2*) and several other sphingolipid-synthesizing enzymes (i.e. *CERS6*, *DEGS2,* and *SGMS1&2*) were upregulated in adenomas (Figures 1C&D), as compared to healthy colon tissue. The increase in *CERS6* was particularly interesting, as it encodes the ceramide synthase isoform that is required to make the C_{16}-ceramides that are signals of nutritional excess [12–15].

We also used quantitative RT-PCR and lipidomics to evaluate the sphingolipid pathway in adenocarcinomas that were surgically removed from colon cancer patients at the Huntsman Cancer Institute at the University of Utah (Table 1). *SPTLC1&2, CERS6, DEGS1&2,* and

SGMS and the sphingolipids C_{16}-ceramides, C_{16}-dihydroceramides, and sphingosine were upregulated in the tumors, as compared to the non-tumorous tissue surrounding the lesion (Figure 1E&1F). The other *CERS* isoforms (1–5)—and the ceramides they produce—were unaltered (Figure 1F, S1B&S1D). The *SGMS* transcripts that encode the sphingomyelin synthases that convert ceramide into sphingomyelin were slightly elevated in the excised tumor, but sphingomyelins were not (Figure 1E and S1D). Other genes that influence ceramide synthesis or metabolism were unaltered (Figure S1B). Thus, the increase in transcripts and sphingolipids was largely restricted to the enzymes in the *de novo* synthesis pathway that produce the C_{16}-ceramides. We also quantified two glycerol-containing lipids (i.e., diacylglycerol and triacylglycerol), finding that they were reduced in the tumors (Figure 1G). This finding suggests that these intestinal tumors redirect fatty acids away from the glycerolipid pathway and towards sphingolipids. As expected, the tumors contained substantially higher levels of *LGR5*, a marker of ISCs (Figure S1C).

High fat diets induce ceramide accumulation in jejunal crypts in mice

To determine whether the sphingolipid pathway in the intestine could be altered by diet, we fed mice either a high-fat diet (HFD, 60% kilocalories from fat) or a low-fat diet (LFD, ~10% kilocalories from fat) for 12 weeks. The obesogenic HFD, which utilizes lard as the primary fat source, increased levels of ceramides in jejunal crypts, but not villi (Figure 1H, left panel). Under these conditions, we didn't observe any overt effects of the HFD on tissue architecture. The increase was observed for several species including C_{16}-, C_{18}-, and C_{24}-ceramides (Figure 1H, right panel). As in the human intestinal samples profiled above, the C_{16}-ceramides were more abundant than other ceramide species. HFD also increased other simple and complex sphingolipids, mainly in the small intestine (Figure S1E).

Excision of *Sptlc2* from mouse intestines disrupts gut architecture and depletes proliferating ISCs

To evaluate the role of sphingolipids in the gut, we produced conditional knockout mice that allow for acute depletion of the *Sptlc2* subunit of SPT from intestinal epithelial cells (IECs). These $Sptlc2^{\delta IEC}$ mice were generated by breeding $Sptlc2^{fl/fl}$ mice that we described previously[16] with mice expressing a tamoxifen inducible Cre-recombinase controlled by the villin promoter (Tg(Vil-cre/ERT2)[17]. Within two days of tamoxifen administration, adult $Sptlc2^{\delta IEC}$ mice displayed a marked reduction in *Sptlc2* mRNA expression in the small intestine and colon as compared to tamoxifen-treated $Sptlc2^{fl/fl}$ littermates (Figure S2A). Deletion of *Sptlc2* led to rapid weight loss (Figure S2B) and death of all animals within 4 days (Figure S2H). Upon necropsy, the $Sptlc2^{\delta IEC}$ mice were found to have a shorter small intestine (Figure S2C & 2D) and a smaller spleen (Figure S2E). The intestine exhibited increased permeability (Figure S2F) and inflammation (Figure S2G). Treatment with broad-spectrum antibiotics prolonged animal survival (Figure S2H), suggesting that sepsis resulting from loss of the intestinal barrier was the ultimate cause of death of the animals.

Biochemical assessment of the intestine revealed that depletion of *Sptlc2* reduced levels of the sphingolipids in the *de novo* synthesis pathway (i.e., ceramides, dihydroceramides, sphinganine, and phytoceramides) within the intestinal crypts (Figure S2I). Surprisingly,

Sptlc2 depletion did not alter levels of complex sphingolipids (i.e., sphingomyelins and glucosylceramides) (Figure S2I). The effects of *Sptlc2* removal manifest predominantly in the crypts, and not in the villi; tamoxifen-treatment affected dihydroceramides, phytoceramides and sphinganine—but not other sphingolipids—within villi of the *Sptlc2*$^{\delta IEC}$ mice (Figure S2J).

Careful histological assessment of the *Sptlc2*$^{\delta IEC}$ mice revealed severe disruption of the small intestine including disorganized villi (Figure 2A, H&E staining) and nearly complete loss of crypts and resident ISCs (Figure 2A, OLFM4 staining). Following the four-day tamoxifen regimen, the *Sptlc2*$^{\delta IEC}$ mice also showed depletion of goblet cells by PAS staining (Figure S2K). Immunohistochemistry with anti-Ki67 antibodies revealed a stark decrease in the rapidly proliferating cells (TA cells) located within the crypt (Figure 2A, Ki67 staining). To identify which cell types were first affected by *Sptlc2* depletion, we conducted a temporal assessment of the changing pathology, collecting the jejunum through each of the first three days following tamoxifen administration. Though the gross epithelial structure of the small intestine in the *Sptlc2*$^{\delta IEC}$ mice remained relatively intact through the first three treatment days, the ISC pool started to disappear within 2-days of tamoxifen injection. This finding was evidenced by reduced expression of OLFM4 (Figure S2L), a disproportionate reduction in the number of crypts (Figure 2B, left), increased apoptosis (Figure S2M) and fewer and mislocalized proliferating cells as assessed by Ki67 staining (Figure 2B, right and Figure S3A).

To further discern which cell types were affected by *Sptlc2* deletion, we conducted droplet-based single-cell 3’ RNA-sequencing of crypts, which were collected two days after tamoxifen administration. We profiled 43,111 crypt cells from *Sptlc2*$^{fl/fl}$ and *Sptlc2*$^{\delta IEC}$ mice. Machine learning identified 10 clusters, which we visualized by t-stochastic neighborhood embedding (tSNE). We could easily identify most of the cell clusters (e.g., stem cells, Paneth cells, enterocytes, goblet cells, enteroendocrine cells, and tuft cells) based on published gene sets [18] (Figure 2C and S3B). In these datasets, we observed marked reduction of *Sptlc2* in stem cells, enterocytes, Paneth and goblet cells (Figure 2). We observed no compensatory changes in *Sptlc1* or *Sptlc3*, nor did we observe changes in the *Ormdl1–3* transcripts that encode the ORMDL proteins, which regulate SPT activity. Several clusters in the middle part of the t-SNE plot—which were positive for *Olfm4* but negative for *Lgr5*—disappeared following *Sptlc2* deletion (Figure 2C, 2D, S3B, and S3C). This group of cells showed moderate to low expression of differentiated cell markers. We thus suspect that these *Sptlc2*-sensitive cells are the rapidly proliferating transit amplifying cells (TACs) that are immediate descendants of ISCs.

Excision of *Sptlc2* from ISCs recapitulates the lethal phenotype of the *Sptlc2*$^{\delta IEC}$ mice

The findings presented thus far suggest that sphingolipids might be autonomous and essential signals that control the proliferation of ISCs to promote epithelial regeneration. Experiments using RNA *in situ* hybridization reinforced this idea, as they revealed that *Sptlc2* transcript levels were much higher in the crypts than they were in the villi (Figure 2F). This observation suggests that the ISCs or TACs within the crypt were the major sites of sphingolipid synthesis and action. This conclusion was corroborated by the lipidomic

assessments showing higher ceramides and phytoceramides in the crypts, as compared to the villi (Figure S4A).

To selectively study the role of sphingolipids in progenitor cells, we generated a mouse line allowing for ISC-specific *Sptlc2* depletion (*Sptlc2*$^{\delta ISC}$) by breeding the *Sptlc2*$^{fl/fl}$ mice with *Olfm4-EGFP-ires-CreERT2* mice[19]. Injecting tamoxifen into the *Sptlc2*$^{\delta ISC}$ mice depleted *Sptlc2* from the crypts, while it was retained in the other cells in the villi (Figure 2F, *Sptlc2* staining). This led to the quick disappearance of the ISCs, as assessed by labeling *Olfm4* using RNA *in situ* hybridization (Figure 2F, *Olfm4* staining). By comparison, *Lyz1*, which demarcates Paneth cells in the crypt, was largely unaffected by *Sptlc2* depletion (Figure 2F, *Lyz1* staining). In these *Sptlc2*$^{\delta ISC}$ mice, tamoxifen also recapitulated the gross phenotype of the *Sptlc2*$^{\delta IEC}$ mice, including the reduction in body weight, rapid death, shortened small intestine and small spleen (Figure S4B–S4F). Histologic analysis showed a comparable disruption of the small intestine structure that was most pronounced in the crypts (Figures S4G and S4H).

We also attempted to deplete *Sptlc2* from *Lgr5*-positive cells, using *Lgr5-EGFP-ires-CreERT2* mice that have been described previously [19]. Depletion of *Sptlc2* from these cells did not alter animal health or viability, nor did it alter the gut structure. This finding is consistent with the single-cell sequencing data, where the *Lgr5*-positive cells remained intact following *Sptlc2* depletion. However, we obtained a mosaic knockout of *Sptlc2*, which disappeared from only a portion of *Lgr5*-positive cells. Because of this heterogenous expression pattern, we cannot definitively conclude that *Lgr5*-positive ISCs are refractory to the effects of *Sptlc2* depletion.

Manipulating sphingolipid synthesis in *Drosophila Melanogaster* alters ISC proliferation

We also investigated whether the sphingolipid synthesis pathway modulates ISC behavior and epithelial homeostasis using *Drosophila Melanogaster*, which has comparable intestinal cell types, cellular functions and cellular interactions as compared to the mammalian intestine. We used RNAi targeting either the SPT homolog *lace* or CERS homolog *schlank* in ISCs, finding they inhibited cell proliferation (Fig. 3A, left), and thus recapitulated the phenotype that we observed following gene depletion in mice. By comparison, we didn't observe changes in proliferation when we removed the genes from enterocytes, enteroendocrine cells, or enteroblasts (Fig. S5). The powerful genetic tools available in *Drosophila* also allowed us to inducibly overexpress the genes in intestinal progenitors, and thus model the consequences of diet-induced induction of the pathway. Introducing either *lace* or *schlank* increased progenitor proliferation (Figure 3A, right). These findings uncover an evolutionarily conserved role for sphingolipids as drivers of progenitor cell proliferation and gut regeneration.

Using a *Drosophila ApcRas* colon cancer model that harbors compound mutations in *Apc* and *Ras* [20], we further evaluated the function of the *de novo* sphingolipid synthesis pathway in formation of tumors. We knocked down either *lace* or *schlank* from *ApcRas* mutant flies using RNAi. Knockdown of *lace* eliminated most of the cancerous *ApcRas* clones (Figure 3B and S4I, left, S5A), while knockdown of *schlank* led to severe reduction in the size of *ApcRas* clones without reducing the number of clones compared to controls

(Figure 3B and S4I, middle & right, S5B). These results suggest that *de novo* sphingolipid synthesis is necessary and sufficient for both the incidence and growth of colorectal cancers in *Drosophila*.

Compared to controls, over expression of lace or schlank in the ISCs, increases the number and size of the ISCs. In the EBs, lace over-expression increases it's numbers without affecting the EB cell morphology (Figure S5C. Schlank o/e in the EBs, however, increases the EB cell size without changing the number of cells (Figure S5C). Lace over-expression in ECs or EEs does not affect the cell morphology or it's numbers (Figure S5C). Schlank o/e ECs on the other hand is associated with loss of EC cells, but no change when over expressed in EEs (Figure S5C). Lace and Schlank knockdown in ISCs, EBs, and ECs are associated with loss of ISCs, but no change in EBs and ECs (Figure S5C). Lace knock-down changes the morphology of the EEs, and increases it's number while schlank knockdown in the EEs have no effect on the cells (Figure S5C).

Ceramides enhance stemness and survival of intestinal organoids

To better understand how SPT regulates stem cells, we turned to an intestinal organoid 3-D culture system [9]. These mini-intestines contain all of the cell types of the mature epithelium but allow for precise control of the tissue environment. Pharmacological inhibition of SPT (i.e., treatment with the SPT inhibitor myriocin) or genetic ablation of *Sptlc2* [i.e., treatment with 4-hydroxytamoxifen (4-OHT)] led to rapid death of the organoids, as assessed by propidium iodide staining (Figure 3C and Figure S6A). Thus, we recapitulated the *in vivo* phenotype caused by *Sptlc2* depletion using this *in vitro* system. Organoid viability could be restored by supplementing with short-chain analogs of ceramide (C_2-ceramide, 25 μM) (Figure 3C and S6A). Mass spectrometry confirmed that treating with this dose of C_2-ceramide restored levels of most sphingolipids in either the myriocin or 4-OHT treated organoids (e.g. ceramides, glucosylceramides, sphingomyelins and sphingosine), excepting those sphingolipids that cannot be reproduced from C_2-ceramide via the salvage pathway (e.g. sphinganine and dihydroceramides) (Figure S6C and S6D). In 4-OHT-treated organoids, removing C_2-ceramide from the media reinitiated the death program (Figure 3C and S6A).

To clarify which sphingolipid species might be important for organoid viability, we exposed these organoid cultures to either the glucosylceramide synthase inhibitor D-threo-et-P4 or the sphingomyelin synthase inhibitor D609, which inhibits the production of glucosylceramides and sphingomyelin, respectively. Neither of these compounds recapitulated the myriocin effects on organoid survival (Figure S6B). By contrast, fumonisin, a pan ceramide synthase inhibitor, induced organoid death (Figure S6B), indicating that de novo pathway is essential for intestinal regeneration. Collectively, these data suggest that intermediates in the *de novo* sphingolipid synthesis pathway (e.g., sphingosine, ceramides or phytoceramides), rather than the abundant complex sphingolipids that comprise the majority of the sphingolipidome (e.g., sphingomyelins), were requisite for organoid viability.

To confirm that C_2-ceramide modulated stemness, we quantified the number of crypt domains per organoid following exposure to C_2-ceramide. As we anticipated, treating the

secondary organoids with C_2-ceramide decreased the number of buds sprouting from each organoid, supporting the idea that sphingolipids enhanced stemness (Figure 3D and S6E, right). C_2-ceramide also increased the number of proliferating cells in the organoids, which were assessed by Edu staining (Figure 3D and S6E, left).

Given the recently identified role for necroptosis in ISCs [21, 22], we investigated the expression of necroptotic genes such as *Rikp3*, *TNF*, *Tnfaip3*, *NfkB2*, and *MLKL* in organoids using qPCR. Several of these genes were upregulated following *Sptlc2* depletion (Figure S6F). The addition of ceramide restored expression of these genes (Figure S6F). These data suggest that inhibition of necroptosis may be an additional mechanism by which sphingolipids promote organoid survival.

Ceramides enhance stemness by stimulating FABP1 expression to increase fatty acid uptake

To explore the molecular mechanism(s) that might account for the profound sphingolipid actions in the intestinal epithelium, we conducted RNA sequencing (RNAseq) on *Sptlc2*-knockout organoids treated with or without C_2-ceramide. As mentioned above, *Fabp1*, which encodes a fatty acid binding protein involved in lipid uptake, was amongst the handful of transcripts most dramatically upregulated by C_2-ceramide (Figure 3E). This C_2-ceramide effect on FABP1 was particularly interesting owing to a bevy of studies showing that saturated fatty acids increase the expression of FABP1 in ISCs [23] and that increasing fatty acid oxidation enhances stemness [5, 23, 24]. *Sptlc2* depletion decreased *Fabp1* transcripts in the crypt, but not the villi (Figure 3F). Using organoids, we confirmed that *Sptlc2* depletion decreased, and C_2-ceramide restored, expression of *Fabp1* mRNA (Figure 3G) and FABP1 protein (Figure 3H and S6G).

To evaluate the functional consequences of SPT and ceramide on lipid handling, we quantified fatty acid uptake in organoids isolated from the $Sptlc2^{\delta IEC}$ mice treated with vehicle, 4OHT, or C_2-ceramide. C_2-ceramide stimulated fatty acid uptake in organoids. By contrast, depletion of *Sptlc2* using 4OHT reduced rates of fatty acid uptake (Figure 3I).

The RNA sequencing data also identified the transcript encoding carnitine palmitoyltransferase-1 (*Cpt1a*), the enzyme that facilitates fatty acid entry into mitochondria, as a C_2-ceramide-responsive gene. We confirmed that C_2-ceramide increased expression of *Cpt1a* transcripts (by qPCR, Figure 4A) and CPT1a protein (by Western blot, Figure 4B). The CPT1 inhibitor etomoxir negated the protective actions of C_2-ceramide on the survival of *Sptlc2* knockout organoids (Figure 3J, and Figure S6H). Thus, induction of fatty acid uptake and utilization were essential C_2-ceramide actions that preserved ISC viability. Interestingly, scRNAseq datasets corroborate this finding that *Sptlc2*-depletion led to a strong downregulation of both *Fabp1* and *Cpt1a* genes in the ISC clusters, as well as markers of proliferation like Mki67 (Figure 2E). Curiously, the expression of these two transcripts was also reduced in Paneth cells (Figure 2E). While we don't know precisely why this is occurring in Paneth cells, we note that under damaged conditions, Paneth cells de-differentiate to replenish the stem cell pool.[25] We anticipate that is happening under these ISC-depleted conditions.

Ceramides increase FABP1 expression through PPARα activation

Prior studies have shown that the transcription factors peroxisome-proliferator activated receptor isoforms alpha (PPARα) and delta (PPARδ) regulate FABP1 expression in the small intestine [26–29]. In addition, recent studies have implicated PPARδ as a critical intermediate linking saturated fats to the control of fatty acid oxidation and the enhancement of ISC stemness [2, 23]. We thus tested whether *Fabp1* or *Cpt1* expression was controlled by either of these transcription factors. The PPARα antagonist GW6471 blocked the C_2-ceramide induction of *Fabp1* (Figure 4A and 4B), but not *Cpt1a*. The PPARδ antagonist GSK3787 had no effect on either gene (Figure 4A). Thus, PPARα, but not PPARδ, was an essential intermediate linking C_2-ceramide to the induction of FABP1.

Lastly, we evaluated whether PPARα was sufficient to maintain organoid viability, even in the absence of *Sptlc2*. The PPARα agonist GW7647 restored the viability of organoids lacking *Sptlc2* (Figure 4C and 4D). GW7647-treated organoids had fewer crypts in each organoid, thus recapitulating the C_2-ceramide effect on organoid stemness (Figure 4E and 4F). Moreover, GW7647 treatment recapitulated the ceramide effect on *Fabp1* expression (Figure 4G). We also confirmed that C_2-ceramide, but not its downstream degradation product sphingosine, increased the binding activity of PPARα to its response element (Figure 4H). These studies convincingly display the existence of a sphingolipid-PPARα-FABP1 axis that links macronutrients to the maintenance of the ISC pool (Figure 4I).

Discussion

These studies provide important mechanistic insight into the nutritional signals that control the metabolism and proliferation of ISCs, the cell-of-origin of gastrointestinal cancers. Prior studies have shown that the transition from normal ISCs into a hyperplastic lesion is dependent upon fuel choice [30]. Excessive fatty acid supply increases the proliferation and stemness of progenitors within the crypt to increase the likelihood of tumor formation [5, 23, 24]. In mouse models, genetic depletion or pharmacological inhibition of the mitochondrial pyruvate carrier—which increases dependence on fatty acid oxidation—expands the ISC compartment and doubles the frequency of adenoma formation [30, 31]. By contrast, germline deletion of *Fabp1* slows lipid uptake and reduces adenoma formation [32]. The findings described herein reveal that ceramides—which are enriched in the crypt and upregulated in mice fed a high fat diet—influence fuel choice by enhancing fatty acid import through FABP1.

Prior studies have shown that genetic ablation of *Sptlc2* [33, 34] or pharmacological inhibition of SPT [35] has deleterious consequences on gut health, with the former causing animal death and the latter gastric enteropathy. Indeed, inflammatory bowel disease has been associated with decreased expression of SPT [33]. The studies described herein indicate that these pathogenic states may result from decreased conversion of free fatty acid and amino acids into ceramides and concomitant depletion of a subtype of intestinal progenitors. In particular, the scRNAseq analysis—which was conducted two days after *Sptlc2* deletion and prior to a major histological change in the gut—revealed a profound loss of $Olfm4^{+}/Lgr5^{-}$ cells. These cells appear to be a subset of progenitors including TACs, as they lack most of the key markers of fully differentiated cell types yet retain the ISC marker *Olfm4*. They

are likely to be immediate descendants of the *Olfm4*$^{+}$/*Lgr5*$^{+}$ ISCs, which showed a dramatic decline in proliferation following *Sptlc2* depletion. These data convincingly demonstrate that proliferation and potentially survival rely heavily on sphingolipid synthesis. Thus, strategies regulating sphingolipids or their targets could prove effective as a means of modulating the health of the intestinal epithelium.

Importantly, under the conditions described herein, these ceramides are produced endogenously within the ISCs via *de novo* synthesis. Recent studies have shown that the microbiome can supply sphingolipids to the host and regulate intestinal homeostasis and symbiosis [36, 37]. In the studies presented herein, bacterially-derived sphingolipids are evidently insufficient to restore ISC health in the *Sptlc2* knockout mice.

We acknowledge that Metallo and colleagues reported that SPT antagonizes cell proliferation [38]. In those studies, conducted under serine-deprived conditions, SPT's inhibitory actions were attributed to its use of the non-preferred substrates alanine and glycine, which produces non-abundant deoxyceramides that impair cell division. Those published data are compatible with our findings, which were conducted in live animals and/or cultured organoids where serine was abundant. Under the more biologically relevant serine replete conditions, SPT produces ceramides which enhance ISC division, but very low levels of inhibitory deoxyceramides (compare Figures 1H and S1D). The studies suggest the existence of a rheostat involving SPT—and ceramides and deoxyceramides—which gauges the availability of amino and fatty acids to either increase or decrease ISC division.

We also acknowledge that ceramides have long-been implicated in apoptosis,[39] which seems unrelated to their actions in the ISC. We previously demonstrated that ceramides altered cell function via a two-stage process [6]. First, they alter the metabolic program to upregulate fatty acid utilization and impair carbohydrate utilization. Second, as ceramides continue to accrue—particularly in the outer mitochondrial membrane—they induce apoptosis. In ISCs, the former seems to predominate, leading to a concomitant change in cellular proliferation rather than induction of cell death. We surmise that this proliferative mechanism occurs before the induction of apoptosis in this unique cell population.

Our data further identify PPARα as an essential intermediate that links endogenous sphingolipids to the induction of *Fabp1*. This is consistent with prior studies, which show that high fat diet increases levels of *Pparα* and its downstream target *Fabp1* in rat jejunum [40], as well as a study showing that a PPARα antagonist induces organoid death [41]. Moreover, it aligns with *in vitro* studies suggesting that sphingolipids may activate PPARα [42–45]. Herein, we define the order of events and determine that these entities participate in a regulatory signaling cascade that dramatically alters ISC proliferation *in vivo*.

We note that PPARα expression is down-regulated in human colon adenocarcinomas [46]. This seems to be a consistent pattern with many of these genes, such as *Fabp1* [32], which are upregulated in adenomas but then downregulated as the tumor progresses to form an adenocarcinoma. Most colorectal cancers involve a stepwise series of events and mutations resulting in a progression of benign adenomas to colorectal cancer. Increased ISC proliferation is an initial and essential step in this process because it increases the chance of

carcinogenesis [47, 48]. After transformation, the transcriptome pattern can be fundamentally altered. Thus, the adenoma stage may be the window when this ceramide-PPARα-FABP1 is significantly upregulated. Our findings indicate that ceramide enhances PPRE binding activity of PPARα and reveal that the ceramide-PPAR-FABP1 axis serves as a signaling pathway to activate fatty acid uptake and oxidation. This alteration in the metabolic program is an essential component of ISC proliferation and expansion, which is a key step in epithelial regeneration. The data obtained thus provides new and important information about the nutritional sensing machinery that induces this transcriptional program to control ISC behaviors.

Collectively, these data support the conclusion that overproduction of sphingolipid enhances stemness of cells within the intestinal crypts. Studies in mice, flies, and organoids reveal that these lipids are potent regulatory signals that drive the expansion of the ISC and TAC pools. Using the organoid system, we then identified an intriguing mechanism linking sphingolipids to the modulation of stemness through their effects on PPARα-mediated induction of FABP1 and a resultant increase in fatty acid uptake. These observations help reveal how saturated fatty acids control intestinal stemness and provide an explanation for the utility of serine deprivation as a means to decrease tumor incidence. Finally, because stem cells play a major role not only in tissue regeneration but also in carcinogenesis, deciphering their response to dietary factors is of utmost importance for the treatment of degenerative conditions. Ultimately, these studies could suggest dietary or pharmacological strategies for maximizing regenerative capacity while also minimizing the risk of cancer development.

Supplementary Material

Refer to Web version on PubMed Central for supplementary material.

Acknowledgements

We wish to acknowledge the support from Metabolomics, Histology, and Metabolic Phenotyping Cores at the Health Sciences Center of the University of Utah. All data are available in the main text or the supplementary materials.

Funding:

Mass spectrometry equipment for the Metabolomics core was obtained through NCRR shared instrumentation grants 1S10OD016232-01, 1S10OD018210-01A1 and 1S10OD021505-01 and microscopy equipment for histology was obtained using a NCRR Shared Equipment Grant # 1S10RR024761-01. Preclinical Research Resource was supported by the National Cancer Institute of the National Institutes of Health under Award Number P30CA042014. The authors received research support from the National Institutes of Health (CA272529, DK115824, DK116888, DK116450, and DK130296 to SAS; DK124326 to B.C; and DK108833 and DK112826 to WLH, F99CA253744 to JAB), the Juvenile Diabetes Research Foundation (JDRF 3-SRA-2019-768-A-B to SAS and JDRF 3-SRA-2019-768-A-B to WLH), the American Diabetes Association (to SAS), the American Heart Association (to SAS), the Margolis Foundation (to SAS), and the United States Department of Agriculture (2019-67018-29250 to B.C.). J.L.W. received support from the National Institutes of Health through the Ruth L. Kirschstein National Research Service Award 5T32DK091317 from the National Institute of Diabetes and Digestive and Kidney Diseases. ZSM is supported from a NIH NHLBI 1T32 HL139451. The content of this manuscript is solely the responsibility of the authors and does not necessarily represent the official views of the National Institutes of Health (NIH).

Data Statement

The authors will provide access to all data collected or resources generated as a part of this research. They will deposit transcriptomic data including RNAseq and single cell analyses into the Gene Expression Omnibus database.

References and Notes

1. Leblond CP, Stevens CE. The constant renewal of the intestinal epithelium in the albino rat. Anat Rec 1948;100:357–77. [PubMed: 18906253]
2. Beyaz S, Mana MD, Roper J, et al. High-fat diet enhances stemness and tumorigenicity of intestinal progenitors. Nature 2016;531:53–8. [PubMed: 26935695]
3. Maddocks ODK, Athineos D, Cheung EC, et al. Modulating the therapeutic response of tumours to dietary serine and glycine starvation. Nature 2017;544:372–376. [PubMed: 28425994]
4. Summers SA, Chaurasia B, Holland WL. Metabolic Messengers: Ceramides. Nature Metabolism 2019;1:1051–1058
5. Bensard CL, Wisidagama DR, Olson KA, et al. Regulation of Tumor Initiation by the Mitochondrial Pyruvate Carrier. Cell Metab 2019.
6. Chaurasia B, Tippetts TS, Mayoral Monibas R, et al. Targeting a ceramide double bond improves insulin resistance and hepatic steatosis. Science 2019;365:386–392. [PubMed: 31273070]
7. Weir JM, Wong G, Barlow CK, et al. Plasma lipid profiling in a large population-based cohort. J Lipid Res 2013;54:2898–908. [PubMed: 23868910]
8. Takahashi N, Vereecke L, Bertrand MJ, et al. RIPK1 ensures intestinal homeostasis by protecting the epithelium against apoptosis. Nature 2014;513:95–9. [PubMed: 25186904]
9. Sato T, Vries RG, Snippert HJ, et al. Single Lgr5 stem cells build crypt-villus structures in vitro without a mesenchymal niche. Nature 2009;459:262–5. [PubMed: 19329995]
10. Sabates-Bellver J, Van der Flier LG, de Palo M, et al. Transcriptome Profile of Human Colorectal Adenomas. Molecular Cancer Research 2007;5:1263–1275. [PubMed: 18171984]
11. Skrzypczak M, Goryca K, Rubel T, et al. Modeling oncogenic signaling in colon tumors by multidirectional analyses of microarray data directed for maximization of analytical reliability. PLoS One 2010;5.
12. Raichur S, Wang ST, Chan PW, et al. CerS2 Haploinsufficiency Inhibits beta-Oxidation and Confers Susceptibility to Diet-Induced Steatohepatitis and Insulin Resistance. Cell Metab 2014;20:919. [PubMed: 29665397]
13. Turpin SM, Nicholls HT, Willmes DM, et al. Obesity-induced CerS6-dependent C16:0 ceramide production promotes weight gain and glucose intolerance. Cell Metab 2014;20:678–86. [PubMed: 25295788]
14. Hammerschmidt P, Ostkotte D, Nolte H, et al. CerS6-Derived Sphingolipids Interact with Mff and Promote Mitochondrial Fragmentation in Obesity. Cell 2019;177:1536–1552 e23. [PubMed: 31150623]
15. Raichur S, Brunner B, Bielohuby M, et al. The role of C16:0 ceramide in the development of obesity and type 2 diabetes: CerS6 inhibition as a novel therapeutic approach. Mol Metab 2019;21:36–50. [PubMed: 30655217]
16. Chaurasia B, Kaddai VA, Lancaster GI, et al. Adipocyte Ceramides Regulate Subcutaneous Adipose Browning, Inflammation, and Metabolism. Cell Metab 2016;24:820–834. [PubMed: 27818258]
17. Goh VJ, Tan JS, Tan BC, et al. Postnatal Deletion of Fat Storage-inducing Transmembrane Protein 2 (FIT2/FITM2) Causes Lethal Enteropathy. J Biol Chem 2015;290:25686–99. [PubMed: 26304121]
18. Haber AL, Biton M, Rogel N, et al. A single-cell survey of the small intestinal epithelium. Nature 2017;551:333–339. [PubMed: 29144463]
19. Schuijers J, van der Flier LG, van Es J, et al. Robust cre-mediated recombination in small intestinal stem cells utilizing the olfm4 locus. Stem Cell Reports 2014;3:234–41. [PubMed: 25254337]

20. Martorell O, Merlos-Suarez A, Campbell K, et al. Conserved mechanisms of tumorigenesis in the Drosophila adult midgut. PLoS One 2014;9:e88413. [PubMed: 24516653]
21. Otsubo K, Maeyashiki C, Nibe Y, et al. Receptor-Interacting Protein Kinase 3 (RIPK3) inhibits autophagic flux during necroptosis in intestinal epithelial cells. FEBS Lett 2020;594:1586–1595. [PubMed: 31997355]
22. Wang R, Li H, Wu J, et al. Gut stem cell necroptosis by genome instability triggers bowel inflammation. Nature 2020;580:386–390. [PubMed: 32296174]
23. Mihaylova MM, Cheng CW, Cao AQ, et al. Fasting Activates Fatty Acid Oxidation to Enhance Intestinal Stem Cell Function during Homeostasis and Aging. Cell Stem Cell 2018;22:769–778 e4. [PubMed: 29727683]
24. Knobloch M, Pilz GA, Ghesquiere B, et al. A Fatty Acid Oxidation-Dependent Metabolic Shift Regulates Adult Neural Stem Cell Activity. Cell Rep 2017;20:2144–2155. [PubMed: 28854364]
25. Yu S, Tong K, Zhao Y, et al. Paneth Cell Multipotency Induced by Notch Activation following Injury. Cell Stem Cell 2018;23:46–59 e5. [PubMed: 29887318]
26. Poirier H, Niot I, Monnot MC, et al. Differential involvement of peroxisome-proliferator-activated receptors alpha and delta in fibrate and fatty-acid-mediated inductions of the gene encoding liver fatty-acid-binding protein in the liver and the small intestine. Biochem J 2001;355:481–8. [PubMed: 11284737]
27. Darimont C, Gradoux N, Cumin F, et al. Differential regulation of intestinal and liver fatty acid-binding proteins in human intestinal cell line (Caco-2): role of collagen. Exp Cell Res 1998;244:441–7. [PubMed: 9806794]
28. Hughes ML, Liu B, Halls ML, et al. Fatty Acid-binding Proteins 1 and 2 Differentially Modulate the Activation of Peroxisome Proliferator-activated Receptor alpha in a Ligand-selective Manner. J Biol Chem 2015;290:13895–906. [PubMed: 25847235]
29. Mochizuki K, Suruga K, Yagi E, et al. The expression of PPAR-associated genes is modulated through postnatal development of PPAR subtypes in the small intestine. Biochim Biophys Acta 2001;1531:68–76. [PubMed: 11278173]
30. Bensard CL, Wisidagama DR, Olson KA, et al. Regulation of Tumor Initiation by the Mitochondrial Pyruvate Carrier. Cell Metab 2020;31:284–300 e7. [PubMed: 31813825]
31. Schell JC, Wisidagama DR, Bensard C, et al. Control of intestinal stem cell function and proliferation by mitochondrial pyruvate metabolism. Nat Cell Biol 2017;19:1027–1036. [PubMed: 28812582]
32. Dharmarajan S, Newberry EP, Montenegro G, et al. Liver fatty acid-binding protein (L-Fabp) modifies intestinal fatty acid composition and adenoma formation in ApcMin/+ mice. Cancer Prev Res (Phila) 2013;6:1026–37. [PubMed: 23921281]
33. Li Z, Kabir I, Tietelman G, et al. Sphingolipid de novo biosynthesis is essential for intestine cell survival and barrier function. Cell Death Dis 2018;9:173. [PubMed: 29415989]
34. Ohta E, Ohira T, Matsue K, et al. Analysis of development of lesions in mice with serine palmitoyltransferase (SPT) deficiency -Sptlc2 conditional knockout mice. Exp Anim 2009;58:515–24. [PubMed: 19897935]
35. Genin MJ, Gonzalez Valcarcel IC, Holloway WG, et al. Imidazopyridine and Pyrazolopiperidine Derivatives as Novel Inhibitors of Serine Palmitoyl Transferase. J Med Chem 2016;59:5904–10. [PubMed: 27213958]
36. Brown EM, Ke X, Hitchcock D, et al. Bacteroides-Derived Sphingolipids Are Critical for Maintaining Intestinal Homeostasis and Symbiosis. Cell Host Microbe 2019;25:668-680.e7.
37. Heaver SL, Johnson EL, Ley RE. Sphingolipids in host-microbial interactions. Curr Opin Microbiol 2018;43:92–99. [PubMed: 29328957]
38. Muthusamy T, Cordes T, Handzlik MK, et al. Serine restriction alters sphingolipid diversity to constrain tumour growth. Nature 2020;586:790–795. [PubMed: 32788725]
39. Obeid LM, Linardic CM, Karolak LA, et al. Programmed cell death induced by ceramide. Science 1993;259:1769–71. [PubMed: 8456305]
40. Suruga K, Mochizuki K, Kitagawa M, et al. Transcriptional regulation of cellular retinol-binding protein, type II gene expression in small intestine by dietary fat. Arch Biochem Biophys 1999;362:159–66. [PubMed: 9917340]

41. Stine RR, Sakers AP, TeSlaa T, et al. PRDM16 Maintains Homeostasis of the Intestinal Epithelium by Controlling Region-Specific Metabolism. Cell Stem Cell 2019;25:830–845 e8. [PubMed: 31564549]
42. Murakami I, Wakasa Y, Yamashita S, et al. Phytoceramide and sphingoid bases derived from brewer's yeast Saccharomyces pastorianus activate peroxisome proliferator-activated receptors. Lipids Health Dis 2011;10:150. [PubMed: 21861924]
43. Van Veldhoven PP, Mannaerts GP, Declercq P, et al. Do sphingoid bases interact with the peroxisome proliferator activated receptor alpha (PPAR-alpha)? Cell Signal 2000;12:475–9. [PubMed: 10989283]
44. Tsuji K, Satoh S, Mitsutake S, et al. Evaluation of synthetic sphingolipid analogs as ligands for peroxisome proliferator-activated receptors. Bioorg Med Chem Lett 2009;19:1643–6. [PubMed: 19237283]
45. Correnti JM, Gottshall L, Lin A, et al. Ethanol and C2 ceramide activate fatty acid oxidation in human hepatoma cells. Sci Rep 2018;8:12923. [PubMed: 30150688]
46. Luo Y, Xie C, Brocker CN, et al. Intestinal PPARα Protects Against Colon Carcinogenesis via Regulation of Methyltransferases DNMT1 and PRMT6. Gastroenterology 2019;157:744–759.e4. [PubMed: 31154022]
47. Barker N, Ridgway RA, van Es JH, et al. Crypt stem cells as the cells-of-origin of intestinal cancer. Nature 2009;457:608–11. [PubMed: 19092804]
48. Drost J, van Jaarsveld RH, Ponsioen B, et al. Sequential cancer mutations in cultured human intestinal stem cells. Nature 2015;521:43–7. [PubMed: 25924068]

What You Need to Know

Background and Context

Obesogenic diets high in saturated fat increase polyp formation and increase gastrointestinal cancer risk.

New Findings

Ceramides, which are products of fat and protein metabolism, accumulate in intestinal adenomas and enhance stem cell proliferation by accelerating fatty acid oxidation.

Limitations

Using preclinical mouse and *Drosophila* models, we demonstrate that ceramides drive stem cell proliferation; however, data in human adenomas are only correlative.

Clinical Research Relevance

These studies suggest that dietary or pharmacological interventions that reduce rates of ceramide synthesis could prevent formation of human adenomas.

Basic Research Relevance

This work reveals a new regulatory axis that allows intestinal stem cells to gauge their nutritional environment and titrate rates of epithelial regeneration. The work has important implications for understanding how progenitors alter fuel choice to modulate their fate.

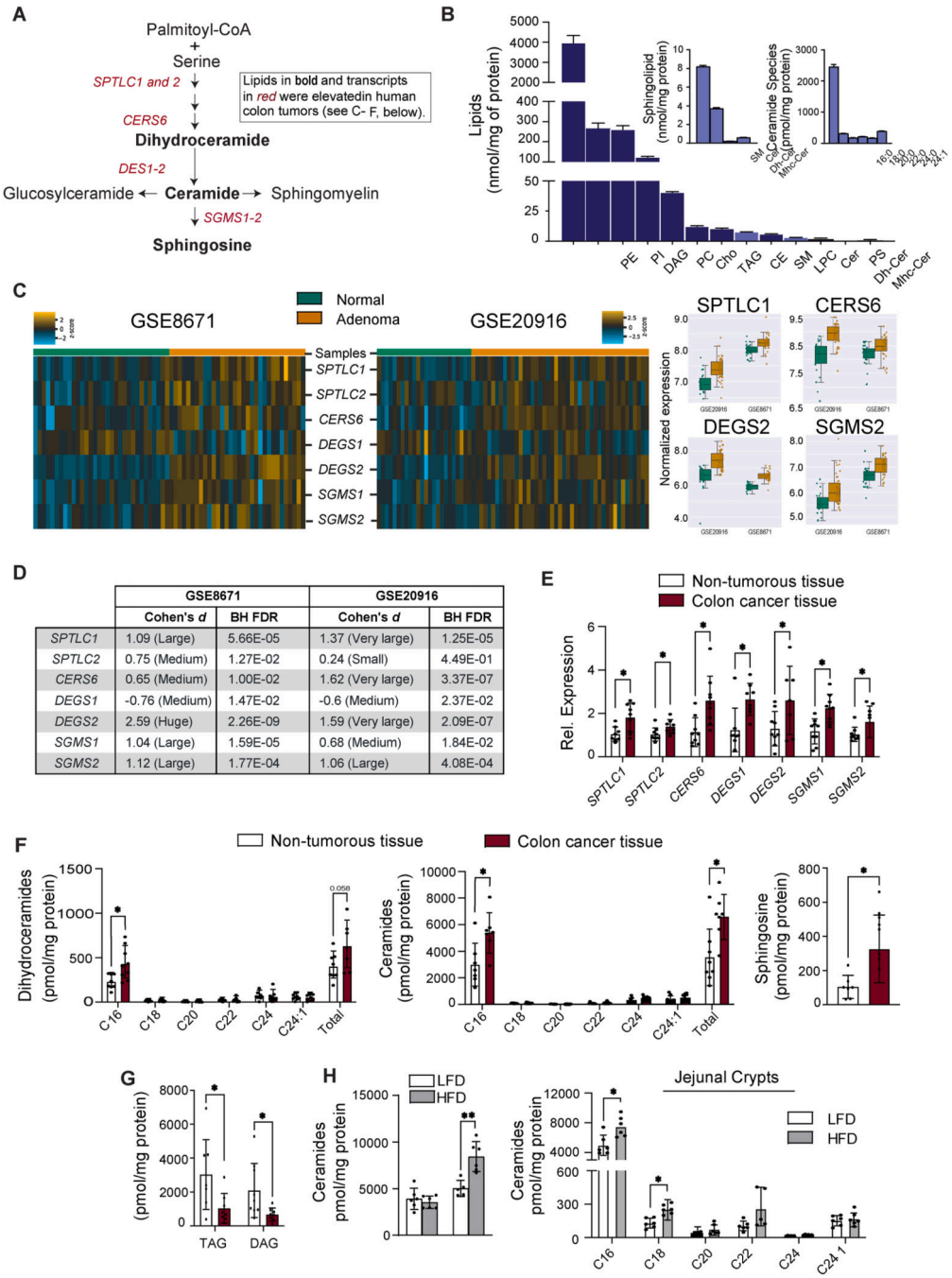

	GSE8671		GSE20916	
	Cohen's *d*	BH FDR	Cohen's *d*	BH FDR
SPTLC1	1.09 (Large)	5.66E-05	1.37 (Very large)	1.25E-05
SPTLC2	0.75 (Medium)	1.27E-02	0.24 (Small)	4.49E-01
CERS6	0.65 (Medium)	1.00E-02	1.62 (Very large)	3.37E-07
DEGS1	-0.76 (Medium)	1.47E-02	-0.6 (Medium)	2.37E-02
DEGS2	2.59 (Huge)	2.26E-09	1.59 (Very large)	2.09E-07
SGMS1	1.04 (Large)	1.59E-05	0.68 (Medium)	1.84E-02
SGMS2	1.12 (Large)	1.77E-04	1.06 (Large)	4.08E-04

Figure 1. Sphingolipids and sphingolipid-synthesizing genes are upregulated in human colon cancer.

(A) Schematic of the sphingolipid synthesis pathway. Shown in bold font are the lipids, and in red font the transcripts, that were upregulated in human colon cancer (see C-F, below). (B) Major lipid species in the mouse small intestine were detected by LC/MS. Sphingolipids are in light blue. (C) Comparison of sphingolipid gene expression in control tissue vs. non-cancer adenoma tissue. Briefly, microarray expression values were z-score scaled and made into a heat map (left). We also included boxplots (right) for 4 genes that have the most significant changes in both data sets. Samples were clustered by

calculating the Euclidean distance between centroids. GSE8671 and GSE20916 samples were assessed against genes probe-set of sphingolipid synthesis. The associated analysis code can be found in this link (https://github.com/j-berg/li_2021). (D) Cohen's effect sizes were used to describe the significance of the gene regulation between normal and non-cancer adenoma tissue. (E) qPCR analysis of transcripts encoding sphingolipid synthesizing enzymes in colon cancer tissue or adjacent non-tumorous tissue obtained from patients. (n=9) (F) Quantification of sphingolipids in colon cancer tissue and adjacent non-tumorous tissue from patients. (n=9) (G) Triacylglycerol and diacylglycerol in colon cancer tissue and adjacent non-tumorous tissue obtained from patients, (n=9). (H) Quantification of sphingolipids in the intestine of C57BL/6 mice fed with a low fat diet (LFD) versus high fat diet (HFD) for 12 weeks. (n=7). (*$p \leq 0.05$, ** $p \leq 0.01$ and ***$p < 0.001$). Abbreviations: PE, phosphatidylethanolamine; PI, phosphatidylinositol; DAG, diacylglycerol; PC, phosphatidylcholine; Cho, cholesterol; TAG, triacylglycerol; CE, cholesterol esthers; SM, sphingomyelin; LPC, lysophosphatidylcholine; Cer, ceramide; PS, phosphatidylserine; Dh-Cer, dihydroceramide; Mhc-Cer, monohexosylceramide; *Sptlc1*, serine palmitoyltransferase long chain base subunit 1; Sptlc2, serine palmitoyltransferase, long chain base subunit 2; *Cers6*, ceramide synthase-6; *Degs1*, dihydroceramide desaturase-1; *Degs2*, dihydroceramide desaturase-2; *Sgms1*, sphingomyelin synthase-1; *Sgms2*, sphingomyelin synthase-2.

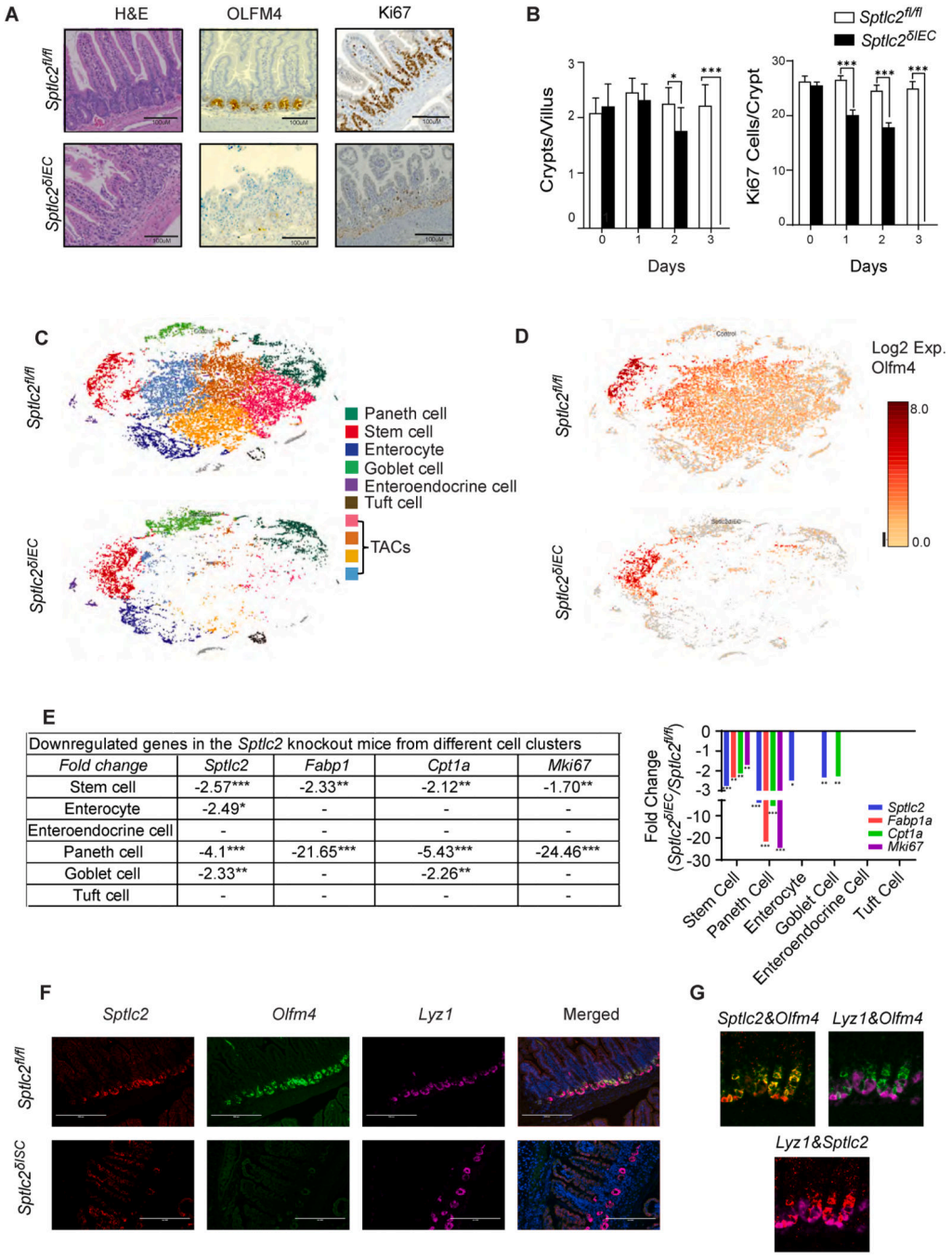

Downregulated genes in the *Sptlc2* knockout mice from different cell clusters

Fold change	*Sptlc2*	*Fabp1*	*Cpt1a*	*Mki67*
Stem cell	-2.57***	-2.33**	-2.12**	-1.70**
Enterocyte	-2.49*	-	-	-
Enteroendocrine cell	-	-	-	-
Paneth cell	-4.1***	-21.65***	-5.43***	-24.46***
Goblet cell	-2.33**	-	-2.26**	-
Tuft cell	-	-	-	-

Fig. 2. Deletion of *Sptlc2* from the intestines disrupts the epithelium and depletes intestinal stem cells.

(A) H&E staining, anti-OLFM4 immunostaning, and anti-Ki67 immunostaining of the jejunum 4-days after intraperitoneal (IP) administration of tamoxifen (1mg/mouse) to *Sptlc2*$^{\delta IEC}$ and *Sptlc2*$^{fl/fl}$ mice. (B) Quantification of crypts per villus or Ki67 positive cells per crypt from *Sptlc2*$^{\delta IEC}$ and *Sptlc*$^{fl/fl}$ mice (n=100). (* p≤0.05, ** p≤0.01 and *** p≤0.001) (C) Identification of crypt-enriched intestinal epithelial cell type clusters from *Sptlc2*$^{\delta IEC}$ and *Sptlc*$^{fl/fl}$ mice by single cell RNA sequencing (tSNE). tSNE plot depicting 22,360 cells from *Sptlc*$^{fl/fl}$ mice and 11,751 cells from *Sptlc2*$^{\delta IEC}$ mice. Cell viability from

the control mouse was 79% and from the knockout mouse was 74.9%. (D) tSNE plot of the expression pattern of *Olfm4* generated with the Loupe Browser (10X Genomics). (E) Downregulated genes in the $Sptlc^{\delta IEC}$ mice from different cell clusters (identified in the single cell RNA sequencing analysis, numbers are the fold change compared to $Sptlc^{fl/fl}$ controls). (F) $Sptlc2^{\delta ISC}$ *and* $Sptlc2^{fl/fl}$ mice were given tamoxifen by intraperitoneal injection (3mg/day for 5 consecutive days). *In situ* hybridization (RNAscope) measuring *Sptlc2*, *Olfm4*, and *Lyz1* mRNA expression was conducted in the intestine on day 5 after tamoxifen injection. Nuclei were stained by DAPI. (G) Samples from the $Sptlc2^{fl/fl}$ mice stained as in F, above, showing combinations of *Sptlc2*&*Olfm4*, *Lyz1*&*Olfm4*, and *Lyz1*&*Sptlc2* stains. Abbreviations: IEC, intestinal epithelia cell; H&E, Hematoxylin and Eosin staining; TACs, transit amplifying cells; *Lyz1*, Lysozyme C1; *Olfm4*, Olfactomedin 4; ISC, intestinal stem cell; serine palmitoyltransferase, long chain base subunit 2; tSNE, t-stochastic neighborhood embedding.

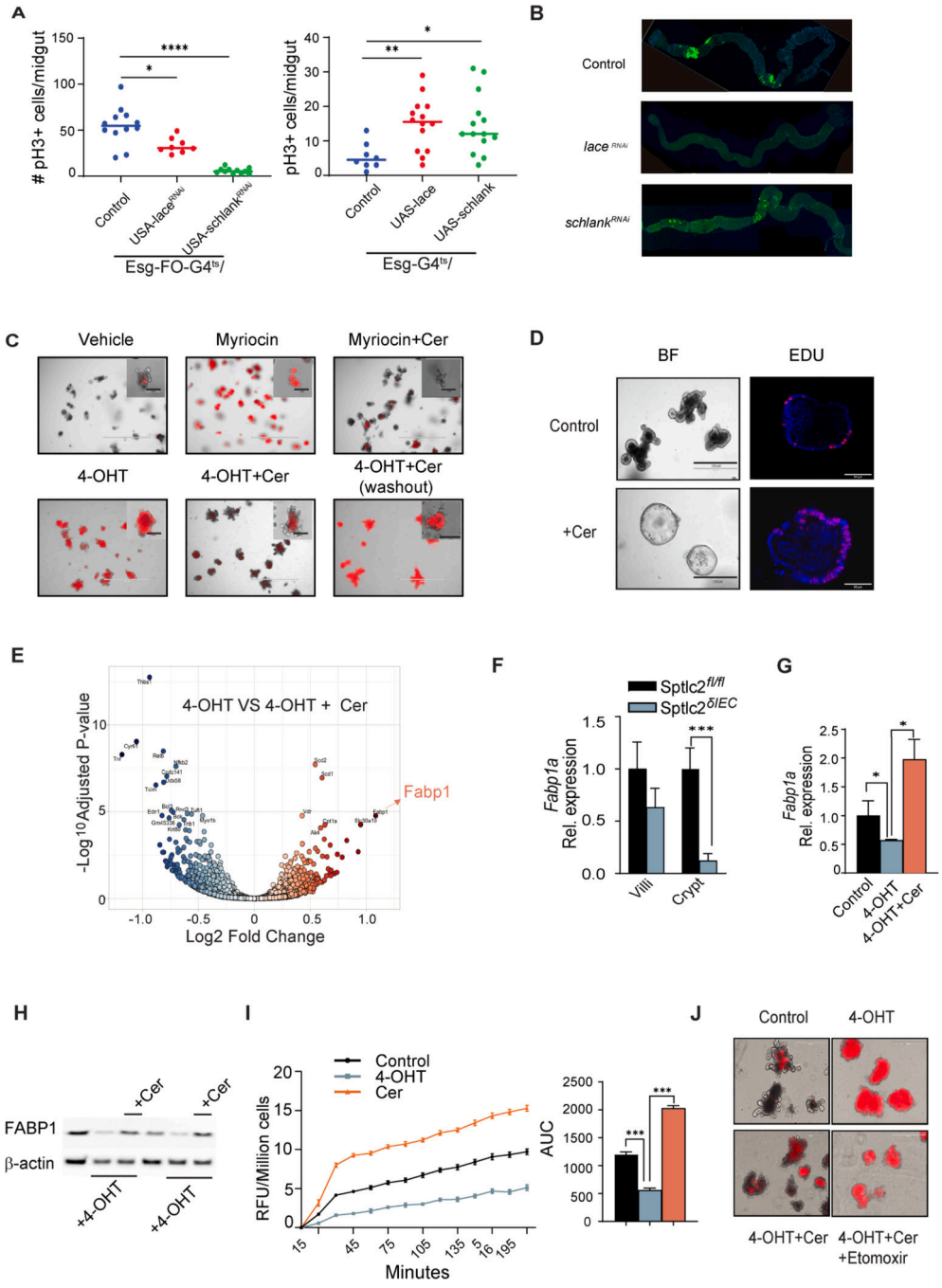

Fig. 3. Ceramides promote stemness and intestinal organoid survival by stimulating FABP1 expression to enhance fatty acid uptake.

Genetic modulation of sphingolipid synthesis genes in the midgut of *Drosophila*: (A) The graph on the left depicts midgut mitosis (pH3+ cells) in control (w1118, n=12) versus *Lace* (n=8) or *Schlank* (n=11) knockdown. Knockdown was controlled by a progenitor-specific and temperature-sensitive Esg-flip out (FO)- Gal4 driver (Esg-FO-G4^{ts}). The graph on the right depicts the quantification of midguts mitosis (pH3+ cells) in control (w1118, n=8) versus *Lace* (n=14) and *Schlank* (n=14) gain-of-function conditions, with transgene expression controlled by a progenitor-specific and temperature-sensitive Esg-Gal4 driver

(Esg-G4^{ts}) (n=50). *denotes p≤0.05, ** p≤0.01 and *** p≤0.001. (B) Panels showing confocal images of the midguts bearing GFP positive *ApcRas* tumor clones at 4 weeks (*n=8,10, 10* for *control, lace*^{KD}, and *schlank*^{KD}). Intestinal organoids were cultured from crypts isolated from the jejunum of *Sptlc*$^{\delta IEC}$ mice. (C) Propidium iodide (PI) staining of organoids treated with either vehicle, myriocin (10μM), or 4OHT (200ng/ml) for 48 hours. Some samples were supplemented with C_2-ceramide (25μM, Cer). In the sample on the lower right, the added C_2-ceramide was then removed from the media (washout) for the final 24 hours. Insets show high magnification images of single organoids. (D) Secondary organoids were treated with either vehicle or C_2-ceramide (25μM) for 7 days. The images on the left show the organoid morphology, while the ones on the right show staining for the proliferation marker EDU. (E) Volcano plot depicting the RNAseq datasets obtained from 4OHT-treated organoids (200 ng/ml) supplemented with or without C_2-ceramide (25μM) for 48 hours. (F) qPCR analysis of *Fabp1* expression in the villi or crypts from the jejuna of the *Sptlc*$^{fl/fl}$ or *Sptlc*$^{\delta IEC}$ mice, respectively. (G) qPCR analysis of *Fabp1* gene expression in organoids treated with vehicle, 4OHT (200 ng/ml), or 4OHT+C_2-ceramide (Cer, 25 μM) for 48 hours. (H) Western blot showing FABP1 and actin expression following *Sptlc2* deletion with 4-OHT and/or C_2-ceramide supplementation for 48 hours. (I) Fatty acid uptake into cells dissociated from organoids that were treated with vehicle, 4OHT, or C_2-ceramide for 48 hours (n=4). The bar graph depicts the area under the curve (3 independent experiments). (J) PI staining images of organoids treated with vehicle, 4OHT, 4OHT plus C2-ceramide or 4OHT plus C2 ceramide plus etomoxir (100μM). Abbreviations: Cer, (d18:1/2:0) N-acetoyl-D-*erythro*-sphingosine; 4-OHT, 4-hydroxytamoxifen; RFU, relative fluorescence unit; IEC, intestinal epithelia cell; FABP1, fatty acid binding protein 1; AUC, area under the curve; Sptlc2, serine palmitoyltransferase; Cpt1a, Carnitine palmitoyltransferase 1A.

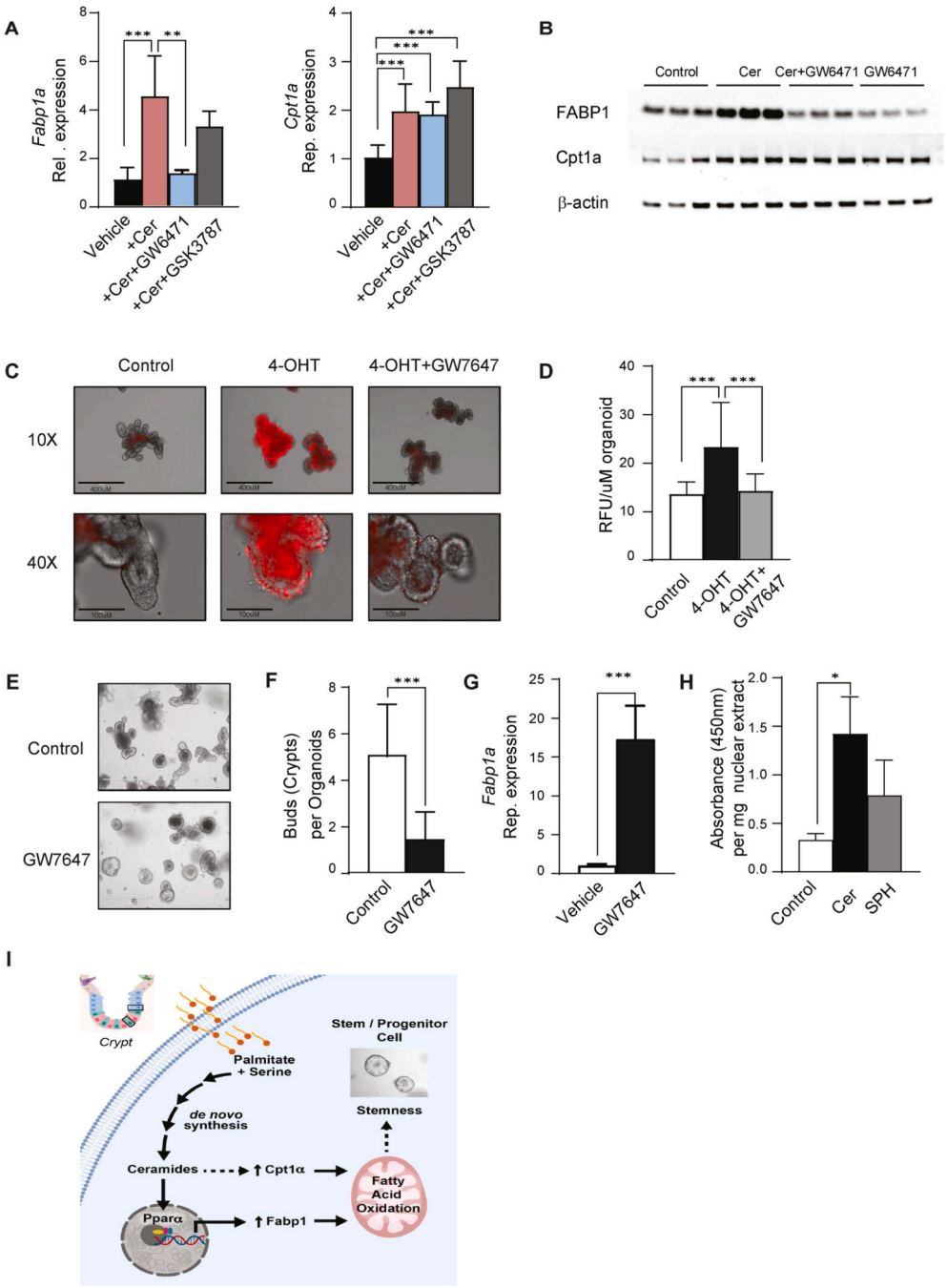

Fig. 4. Ceramides increase FABP1 expression through PPARα activation.

(A) qPCR analysis of *Fabp1* and *Cpt1a* expression in organoids treated with vehicle, C2-ceramide (25 μM), and C_2-ceramide with GW6471(PPARα antagonist, 1μM) or GSK3787 (PPARδ antagonist, 1μM) for 48 hours. (B) Western blot analysis of FABP1, CPT1a, and actin in organoids treated with C_2-ceramide with or without the PPARα antagonist GW6471(GW6471, 1μM) for 48 hours. (C) Propidium iodide (PI) staining of organoids treated with either vehicle, 4OHT (200ng/ml) or 4OHT with the PPARα agonist GW7647 for 48 hours. (D) Quantification of PI staining of 4C (3 independent experiments). (E)

Secondary organoids treated with either vehicle or GW7647 (1μM) for 7 days. (F) Quantification of (E), the crypts growing from each organoid. (n=50, *p<0.05, **p<0.01, ***p<0.001). (G) qPCR analysis of *Fabp1* expression in organoids treated with either vehicle or GW7647 (1μM). (H) Quantification of PPRE binding activity of PPARα in nuclear extracts from organoids treated with vehicle (Control), C2 ceramide (Cer, 25 μM) and sphingosine (SPH, 25μM) for 48 hours. (n=4, *p≤0.05). (I) Schematic depicting the major conclusion of the paper, including the regulatory events that link exogenous palmitate to the regulation of stemness through a ceramide-PPARα-FABP1 axis. Abbreviations: Cer, (d18:1/2:0) N-acetoyl-D-*erythro*-sphingosine; 4-OHT, 4-hydroxytamoxifen; RFU, relative fluorescence unit; IEC, intestinal epithelia cell; FABP1, fatty acid binding protein 1; Cpt1a, Carnitine palmitoyltransferase 1A; PPARα, Peroxisome proliferator-activated receptor alpha; AUC, area under the curve; OD, optical density; FAO, fatty acid oxidation; PPRE, peroxisome proliferator hormone response elements.

Table 1:

Patient information

	Sex	Age	BMI	Hemoglobin (g/dl)	Primary Tumor (tumor depth)	Histologic Type	Histologic Grade
Mean		68.56	26.33	11.88		Ad	
Range		50–84	21.3–34.4	7.6–15.1		Ad	
1	M	61	34.4	12.9	pT3	Ad	Moderately Diff.
2	M	84	23.3	15.1	pT2	Ad	Well to Moderately Diff.
3	M	81	23.25	14.6	pT3	Ad	Moderately Diff.
4	M	50	30.3	10.8	pT3	Ad	Moderately Diff.
5	F	50	22.9	10.3	pT2	Ad	Well Diff.
6	F	58	27.6	10.7	pT4a	Ad	Well Diff.
7	F	80	21.3	12.3	pT2	Ad	Moderately Diff.
8	F	74	30.4	12.6	pT3	Ad	Well Diff.
9	M	79	23.5	7.6	pT3	Ad	Moderately Diff.

Ad: Adenocarcinoma.